Acta Pharmaceutica Sinica B 2020;10(4):693−710

Chinese Pharmaceutical Association
Institute of Materia Medica, Chinese Academy of Medical Sciences

Acta Pharmaceutica Sinica B

www.elsevier.com/locate/apsb
www.sciencedirect.com

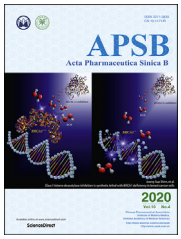

ORIGINAL ARTICLE

Targeted delivery of hyaluronic acid nanomicelles to hepatic stellate cells in hepatic fibrosis rats

Wenhao Li, Chuchu Zhou, Yao Fu, Tijia Chen, Xing Liu, Zhirong Zhang, Tao Gong*

Key Laboratory of Drug-Targeting and Drug Delivery System of the Education Ministry, Sichuan Engineering Laboratory for Plant-Sourced Drug and Sichuan Research Center for Drug Precision Industrial Technology, West China School of Pharmacy, Sichuan University, Chengdu 610064, China

Received 4 May 2019; received in revised form 1 July 2019; accepted 2 July 2019

KEY WORDS

Nanomicelles;
Hyaluronic acid;
Hepatic stellate cells;
Hepatic fibrosis;
Silibinin

Abstract Hepatic fibrosis is one kind of liver diseases with a high mortality rate and incidence. The activation and proliferation of hepatic stellate cells (HSCs) is the most fundamental reason of hepatic fibrosis. There are no specific and effective drug delivery carriers for the treatment of hepatic fibrosis at present. We found that when hepatic fibrosis occurs, the expression of CD44 receptors on the surface of HSCs is significantly increased. Based on this finding, we designed silibinin-loaded hyaluronic acid (SLB-HA) micelles to achieve the treatment of hepatic fibrosis. Meanwhile, we constructed liver fibrosis rat model using Sprague−Dawley rats. We demonstrated that HA micelles had specific uptake to HSCs *in vitro* while avoiding the distribution in normal liver cells and the phagocytosis of macrophages. Importantly, HA micelles showed a significant liver targeting effect *in vivo*, especially in fibrotic liver which highly expressed CD44 receptors. In addition, SLB-HA micelles could selectively kill activated HSCs, having an excellent anti-hepatic fibrosis effect *in vivo* and a significant sustained release effect, and also had a good biological safety and biocompatibility. Overall, HA micelles represented a novel nanomicelle system which showed great potentiality in anti-hepatic fibrosis drugs delivery.

*Corresponding author. Tel./fax: +86 028 85501615.
E-mail address: gongtaoy@126.com (Tao Gong).

Peer review under the responsibility of Chinese Pharmaceutical Association and Institute of Materia Medica, Chinese Academy of Medical Sciences.

https://doi.org/10.1016/j.apsb.2019.07.003

1. Introduction

Liver is a very important organ in the body consisting of hepatic parenchymal cells (HPCs, about 60%−70%) and non-parenchymal cells (about 30%−40%). Among them, non-parenchymal cells include macrophages, Kupffer cells, hepatic stellate cells (HSCs), liver sinusoidal endothelial cells (LSECs), immune cells and other non-parenchymal cells[1]. As the largest solid organ, liver has many physiological functions such as clearing foreign materials, metabolizing drugs, filtering the blood and producing proteins (like albumin)[2−5]. In these, non-parenchymal cells play a crucial role in the liver although their number is so small. For example, Kupffer cells are a kind of macrophages and they are responsible for phagocytic activity[6]. LSECs create the Disse Space and are associated with immune tolerance[7]. HSCs can be activated sometimes, which indicates liver damage[8,9]. Many factors can cause liver diseases such as bacterial invasion, viral infections, physical and chemical changes[10]. In these diseases, hepatic fibrosis is a chronic one which has a high incidence and mortality in the world. The main causes of hepatic fibrosis are alcohol abuse, chronic hepatitis, steatohepatitis and biliary problems. The final pathway of these inducements was fibrotic process[11,12]. Liver fibrosis will gradually develop into cirrhosis and become liver cancer eventually without timely and effective treatment[13].

The occurrence of hepatic fibrosis is closely related to the state of HSCs[14,15]. HSCs are a kind of resident perisinusoidal cells in the Disse Space of liver. The main functions of HSCs are the storage of fat, vitamin A metabolism, synthesis and secretion of important proteins and enzymes[16]. What's more, HSCs are the main cells that secrete collagen and extracellular matrix (ECM), which are directly related to the occurrence of hepatic fibrosis[17]. When the liver is injured by exogenous damage or endogenous inflammation, HSCs will be activated and transformed to be proliferative. Activated HSCs will secrete large amounts of collagen and ECM which could accumulate in the Disse Space and lead to hepatic fibrosis eventually[18]. Therefore, inhibiting the activation of HSCs is a fundamental method for the treatment of hepatic fibrosis. It is gratifying that hepatic fibrosis has been proved to be a reversible process in the past decade[19,20]. Moreover, lots of anti-hepatic fibrosis drugs have been demonstrated to be effective in reversing the activation of HSCs, such as silibinin (SLB), interferon, and small interfering RNA (siRNA)[21,22]. However, it is still difficult to treat hepatic fibrosis currently, mainly for three reasons. The first reason is that HSCs are scarce and they reside in the Disse Space adjacent to LSECs. This physiological location provides a barrier for distributing drugs to HSCs and drugs are more easily internalized by Kupffer cells and LSECs before they reach the HSCs[23]. The second reason is that the surfaces of LSECs exist many small holes with an average diameter of 100 nm[7]. The particle size of drug carrier must be small enough (<100 nm) to allow itself pass through these small holes and further reaching HSCs. The last reason is that most drug delivery systems for the treatment of hepatic disease cannot guarantee the specificity to target liver cells. For example, Zhang et al.[24] designed hepatitis B virus peptide (HBVP)-modified PEGylated liposomes which were used to target HPCs to treat hepatitis. However, their results indicated that the liposomes could also be captured by non-parenchymal cells. The indiscriminate targeting of drugs will damage normal cells. Therefore, it is very important to design an HSC-targeting drug delivery system with high specificity and targeting efficiency for the treatment of hepatic fibrosis.

Hyaluronic acid (HA) is a kind of polysaccharides which is the major constituent of ECM[25,26]. As an endogenous substance, HA is considered as a biodegradable, biocompatible, non-immunogenic and non-toxic biomaterial[27,28]. HA can specifically bind to CD44 receptors which are overexpressed on the surface of various tumor cells[29−31]. Therefore, many researchers have focused on the tumor targeting applications of HA for anticancer therapeutics[32−34]. However, not only tumors, other organs of the body can also express CD44 such as liver, kidney and spleen. But they are less expressed in normal state[35,36]. HSCs are the main cells which express CD44 in the liver. Especially, when hepatic fibrosis occurs, the proliferation of HSCs is accompanied by a significant increase in the expression of CD44[37]. This special physiological phenomenon provides a theoretical basis for the treatment of hepatic fibrosis by using HA as a targeting carrier. Chen et al.[38] designed curcumin-encapsulated HA-polylactic acid (PLA) nanoparticles which were used to target HSCs to treat hepatic fibrosis. However, the particle size of HA-PLA nanoparticles was still large (60−70 nm) and the therapeutic effect needs to be improved. In addition, this research only evaluated the cytotoxicity and pharmacodynamics, and the research contents were relatively insufficient and lacked sufficient persuasiveness. Therefore, the construction of a HSCs targeting vector with smaller particle size and better therapeutic effect, and comprehensive research on it have become our research purposes.

In recent years, nanomicelles have been widely used as drug delivery carriers due to their small particle size, excellent stability and wide drug loading range[39,40]. Among them, the application of phospholipid bile salt micelles is more extensive because of their outstanding ability to dissolve water-insoluble drugs[41]. In this study, we aimed to prepare a kind of SLB-loaded HA-based nanomicelles to achieve HSC-targeted therapy. The partial side chains (COOH−) of HA were modified with deoxycholic acid (DOCA) by using ethylenediamine as the linking group in order to obtain amphipathic HA conjugate. The modified degree of HA conjugate was less than 25% (mol/mol), which were mainly distributed to the liver[42−44]. On the basis of the phospholipid bile salt micelles (Fig. 1A), HA conjugate was used to fabricate HA-functionalized nanomicelles (HA micelles). The hydrophobic side chains of HA conjugate inserted into the hydrophobic core of micelles and the hydrophilic main chains wrapped around the surface of micelles to achieve HSCs targeting (Fig. 1B). The particle size of HA micelles was controlled below 100 nm to ensure that they can pass through small holes in LSECs to reach HSCs. Fig. 1C shows our strategic illustration for the application of HA micelles to target HSCs for the treatment of hepatic fibrosis. SLB could be easily encapsulated into micelles due to its water insoluble effect. *In vitro*, different liver cells were used to study the targeting efficiency of HA micelles. *In vivo*, normal rats and liver fibrosis rats were used to evaluate blood circulation time, liver distribution, HSCs targeting, anti-hepatic fibrosis efficacy and systemic toxicity of HA micelles.

2. Materials and methods

2.1. Materials

Sodium hyaluronate was purchased from Shandong Freda Biopharm Co., Ltd. (Shandong, China). SLB, 3-(4,5-dimethyl-

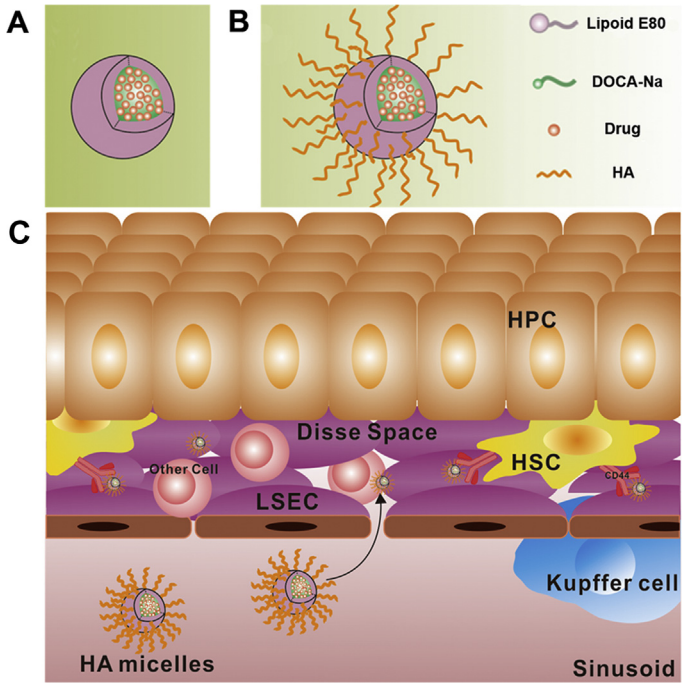

Figure 1 (A) Phospholipid bile salt micelles and (B) HA micelles fabrication. (C) Strategic illustration for the application of HA micelles to target HSCs.

2-thiazolyl)-2,5-diphenyl-2-*H*-tetrazolium bromide (MTT), 1,1′-dioctadecyl-3,3,3′,3′-tetramethylindodicarbocyanine perchlorate (DiD), coumarin 6 (C6) and 4′,6-diamidino-2-phenylindole (DAPI) were purchased from Sigma−Aldrich Shanghai Trading Co., Ltd. (Shanghai, China). Lipoid E80 was purchased from Lipoid Co., Ltd. (Ludwigshafen, Germany). Sodium deoxycholate was obtained from Biosharp Chemical Company (Chengdu, China). *N*-Hydroxysuccinimide (NHS), dicyclohexylcarbodiimide (DCC) and 1-ethyl-3-(3-dimethylaminopropyl)-carbodiimide hydrochloride (EDC) were purchased from Kelong Chemical Company (Chengdu, China). Other chemicals and reagents were analytical grade and obtained commercially.

Sprague−Dawley (SD) rats were purchased from experiment animal center of Sichuan University (Chengdu, China). All animal experiments were performed in accordance with the principles of care and use of laboratory animals and were approved by the ethics committee of Sichuan University.

2.2. *Synthesis of hyaluronic acid-deoxycholic acid (HA−DOCA) conjugate*

Deoxycholic acid-modified HA was synthesized by using ethylenediamine as the linking group (Scheme 1). Briefly, 1.77 g of sodium deoxycholate (4.5 mmol) was dissolved in tetrahydrofuran (THF, 30 mL). DCC (5.4 mmol) and NHS (5.4 mmol) were added to the above solution and stirred for 12 h to activate the carboxyl groups of sodium deoxycholate. Next, the insoluble matters were removed by filtration and the filtrate was precipitated by *n*-hexane to obtain carboxyl activated DOCA. Finally, products were collected and dried, then stored at −20 °C until further use. Aminated DOCA (DOCA−NH_2) was synthesized by amide reaction. Briefly, 0.5 g of DOCA (0.96 mmol) was dissolved in dimethylformamide (DMF, 5 mL) and the solution was slowly dropped to ethylenediamine (8 mL, 0.12 mol), then stirred for 6 h. Next, the reaction solution was precipitated by excess distilled water to obtain DOCA−NH_2. Finally, products were collected and dried.

HA−DOCA was prepared by the following process. First, 0.02 g of HA (MW 100 K, 0.05 mmol) was dissolved in formamide (20 mL) and 0.8 g of DOCA−NH_2 (1.8 mmol) was dissolved in DMF (20 mL). 0.15 g of EDC (0.8 mmol) was added to HA solution and stirred to make full reaction. Next, DOCA−NH_2 solution was added to the above solution and stirred for 24 h. Finally, the reaction solution was dialyzed and lyophilized to obtain HA−DOCA.

2.3. *Characterization of HA−DOCA*

Hydrogen nuclear magnetic resonance (^{1}H NMR) spectra of HA−DOCA were acquired on a Varian spectrometer (FT-80A, Varian, USA). HA−DOCA was dissolved in dimethyl sulfoxide (DMSO) and HA was dissolved in D_2O. The substituting degree of HA−DOCA was estimated using ^{1}H NMR[45].

2.4. *Preparation and characterization of micelles*

2.4.1. *Preparation of HA micelles*

To prepare HA micelles, 23 mg of lipoid E80, 31 mg of sodium deoxycholate and 7 mg of HA−DOCA were dissolved in 5 mL ethanol. HA−DOCA was not soluble in ethanol, but it was enough to disperse uniformly. The solution was dried to a thin film under rotary evaporation and the film was hydrated in 5 mL of phosphate buffer solution (PBS) to obtain HA micelles suspensions. The particle size of HA micelles would become more uniform after homogenization (AH 100D, ATS Engineering Inc., Canada). Meanwhile, we prepared common micelles without HA−DOCA as a control.

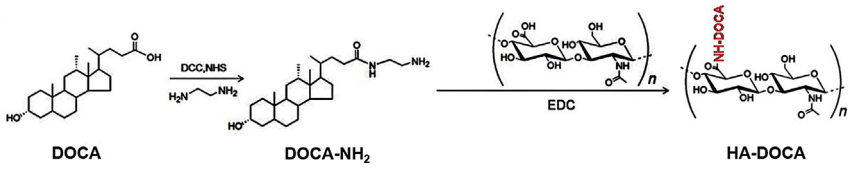

Scheme 1 Synthetic scheme of HA−DOCA conjugate.

2.4.2. *Characterization of HA micelles*

The particle size and zeta potential of HA micelles were measured by dynamic light scattering (DLS) (Zetasizer Nano ZS90, Malvern, UK). The morphology of HA micelles was examined by transmission electron microscopy (TEM, H-600, Hitachi, Japan) with 2% phosphotungstic acid staining.

The critical micelle concentration (CMC) of HA micelles was evaluated by fluorescence spectroscopy (Thermo Scientific Varioskan Flash, Thermo Fisher Scientific, USA), using pyrene as the probe[46]. Briefly, 0.1 mL of 4.0×10^{-3} mol/L pyrene solution in acetone was added to a series of 5 mL volumetric flasks and then acetone was evaporated. 5 mL of different concentrations of HA micelles solutions (5.3×10^{-4} to 2.65 mg/mL) was added to volumetric flasks followed by sonicating for 30 min. All samples were incubated at 37 °C for 24 h. Fluorescence spectra of pyrene was obtained by using fluorescence spectroscopy with an excitation wavelength of 336 nm and emission wavelength of 372 and 383 nm. The CMC was estimated as the knee point when extrapolating the intensity ratio I_{372}/I_{336} at high and low concentration regions.

To research the stability of HA micelles, HA micelles suspensions were separately placed in PBS (pH 7.4) and serum. Particle size change was recorded at intervals[47]. Briefly, 1 mL of the micelles suspensions was added to 4 mL of PBS solution (pH 7.4) or rat serum, and placed at 37 °C with shaking. The particle size was measured at intervals to investigate the stability of the micelles in PBS or serum.

2.4.3. *Preparation of SLB-loaded HA micelles (SLB-HA micelles)*

To prepare SLB-HA micelles, 23 mg of lipoid E80, 31 mg of sodium deoxycholate, 7 mg of HA−DOCA and 4 mg of SLB were dissolved in 5 mL ethanol. The solution was dried to a thin film under rotary evaporation and the film was hydrated in 5 mL of PBS to obtain SLB-HA micelles solution. Meanwhile, we prepared common SLB-loaded micelles (SLB micelles) without HA−DOCA as a control.

Fluorescein (DiD and C6)-loaded micelles and HA micelles were prepared using the same method.

The drug loading capacity (DL) and the entrapment efficiency (EE) were calculated according to the following Eqs. (1) and (2)[48]:

$$\text{DL}\ (\%, w/w) = \text{Weight of loaded drug/Weight of micelles} \times 100 \quad (1)$$

$$\text{EE}\ (\%, w/w) = \text{Weight of loaded drug/Weight of feeding drug} \times 100 \quad (2)$$

2.4.4. *Preparation of SLB solution*

Free SLB solution was prepared by forming a water-soluble double salt with meglumine and SLB. The preparation process was as follows: 40 mg of SLB and 30 mg of meglumine were added to 50 mL of absolute ethanol, and the reaction was stirred at 40 °C for 30 min. After the reaction completed, the solvent was removed by rotary evaporation and the film was dissolved with 5% aqueous solution of glucose to obtain free SLB solution[49].

2.5. *In vitro release*

The *in vitro* release of SLB from SLB micelles and SLB-HA micelles was measured using dialysis bag method[50]. Briefly, 1.0 mL of SLB micelles, SLB-HA micelles and free SLB solution were respectively placed into dialysis bags (3500 Da). Next, the dialysis bags were immersed into 100 mL of PBS containing 0.2% (*w*/*v*) Tween 80 and gently shaken at 37 °C in a shaker (QZX-C, Harbin, China) at 100 rpm. 5.0 mL of release medium was taken out and replaced with 5.0 mL of fresh medium at desired time intervals. The amount of released SLB was measured using high performance liquid chromatography (HPLC) analysis (Agilent 6410, Agilent Technologies, USA)[51].

2.6. *Cell cultures and in vitro cellular uptake study*

The human HSCs ($CD44^+$), human hepatoma cells (HepG2, $CD44^+$), human normal liver cells (LO2, $CD44^-$) and macrophages (RAW 264.7, $CD44^-$) were cultured at 37 °C in a 5% CO_2 atmosphere using Dulbecco's modified Eagle's medium (DMEM) supplemented with 10% fetal bovine serum (FBS), streptomycin (50 U/mL) and penicillin (50 U/mL).

HSCs, HepG2, LO2 and RAW cells were cultured in 12-well plates at a seeding density of 1×10^5 cells/well and incubated for 24 h. Subsequently, the original medium was replaced with DMEM containing DiD solution, DiD micelles and DiD-HA micelles (final DiD concentration was 2 μg/mL). The cells were incubated for 4 h at 37 °C and washed three times with PBS. Next, cells were resuspended and centrifuged at 2000 rpm (refrigerated centrifuge, Allegra X-22R, Beckman Coulter, USA, the same below) for 3 min. The supernatants were discarded and the cells were washed three times with PBS. After centrifugation, cells were resuspended in 0.3 mL of PBS and the fluorescent intensity of cells was measured by flow cytometer (Cytomics™ FC 500, Beckman Coulter, USA). In addition, the cellular uptake mechanism was researched in the presence of free HA (100 kDa, 10 mg/mL). LO2 cells were served as a negative control cell line with no CD44 receptor expression.

The *in vitro* cellular uptake profile of HA micelles was evaluated in HSCs, HepG2, LO2 cells and RAW cells by confocal laser scanning microscopy (CLSM, FV1000, Olympus, USA). Cells were seeded on coverslips and the following step was consistent with the cellular uptake experiments. After 4 h of cell uptake, cells were washed three times with PBS and fixed with 4% paraformaldehyde for 10 min. The cytoskeletons were stained with fluorescein isothiocyante (FITC)-labeled phalloidin for

20 min and the cell nuclei were stained with DAPI for 5 min. Finally, cells were viewed with CLSM.

2.7. Construction of liver fibrosis rat model

Liver fibrosis rat model was induced by intraperitoneal injection of CCl_4 dissolved in soybean oil (2:3, *v/v*). Dosage was 0.5 mL/kg body weight and twice a week for 8 weeks[52]. After 8 weeks, rats were sacrificed and livers were excised. Liver tissues were processed for hematoxylin-eosin (H&E) stain and Masson stain to evaluate the degree of fibrosis.

2.8. Isolation of HPCs, HSCs and other non-parenchymal cells

HPCs, HSCs and other non-parenchymal cells were isolated from normal liver and fibrotic liver using hepatic portal vein catheterization perfusion method[53]. Briefly, a rat was anesthetized with pentobarbital sodium and a midline incision was created in the abdomen of the rat. Then, the hepatic portal vein was cannulated with detaining needle and the liver was perfused with Hanks' balanced salt (HBS) buffer. Five minutes later, the liver was perfused with HBS containing 3 mmol/L $CaCl_2$, 0.05% collagenase IV and 0.01% DNase at 37 °C. After the perfusion, the liver was excised and minced immediately. Next, the tissue was suspended with HBS containing 0.05% collagenase IV and 0.01% DNase at 37 °C, and then filtered with 100 μm screen mesh. Cell suspension was centrifuged at 600 rpm for 8 min and the sediments were HPCs. The supernatant was centrifuged at 2000 rpm for 10 min. The sediments were other non-parenchymal cells and the supernatant was rich in HSCs. Cell viability was estimated using trypan blue staining method.

2.9. Expression of CD44 receptor in HPCs, HSCs and other liver cells

In order to investigate the expression of CD44 receptor in different liver cells and the differences of CD44 receptor expression in normal liver and fibrotic liver, we stained the cells with FITC-labeled CD44 antibody. Briefly, HPCs, HSCs and other non-parenchymal cells were isolated from normal liver and fibrotic liver using the above method. Cell suspensions were centrifuged at 3000 rpm for 5 min and the supernatants were discarded. 100 μL of FITC-labeled CD44 antibody (1:100, diluted with PBS) was added into each tube and cells were incubated for 30 min at 4 °C. Then, cells were centrifuged at 3000 rpm for 5 min, the supernatants were discarded and the cells were washed three times with PBS. Finally, cells were resuspended in 0.3 mL of PBS and the fluorescent intensity of cells was measured by flow cytometer.

2.10. Cytotoxicity assay

In vitro cytotoxicity was evaluated by MTT assay. Activated HSCs, normal HSCs and LO2 cells were cultured in 96-well plates at a seeding density of 1×10^4 cells/well in DMEM medium, then incubated at 37 °C in a 5% CO_2 atmosphere for 24 h. The original medium was replaced with fresh medium containing SLB solution, SLB micelles and SLB-HA micelles (SLB concentrations were from 1.0 to 50.0 μg/mL), then incubated for 48 h. At the same time, we set up blank HA micelles group to eliminate the toxic interference of micelles themselves. Next, 20 μL of MTT solution (5 mg/mL) was added into each well and cells were further incubated for 4 h at 37 °C. The medium was removed and 150 μL of DMSO was added to each well. The optical density was measured using a microplate reader (Thermo Scientific Varioskan Flash, Thermo Fisher Scientific, USA) at 490 nm. Cell viability (%) was calculated according to Eq. (3):

$$\text{Cell viability (\%)} = A_{\text{test}}/A_{\text{control}} \times 100 \quad (3)$$

where A_{test} and A_{control} represent the optical density of cells treated with test samples and culture medium, respectively.

2.11. Pharmacokinetics

SD rats (200−220 g) were randomly divided into three groups ($n = 5$). SLB solution, SLB micelles and SLB-HA micelles were administered intravenously (SLB concentration was 10 mg/kg). Then, 200 μL of blood were collected at predetermined time points (5, 15, 30, 60, 120, 240, 480 and 720 min) after injection[54]. The concentrations of SLB were determined by HPLC. Briefly, 100 μL of plasma sample was extracted with 1 mL of ether and vortexed for 10 min, and then centrifuged at 6000 rpm for 5 min. Then the supernatant was collected and dried with nitrogen. The remains were dissolved with 100 μL of acetonitrile and determined by HPLC[55].

2.12. Biodistribution

Normal SD rats were randomly divided into three groups ($n = 5$). DiD solution, DiD micelles and DiD-HA micelles were administered intravenously (DiD concentration was 10 μg/kg). At 0.25, 1 and 2 h after administration, the rats were sacrificed, and then the major organs (heart, lung, spleen, liver, and kidney) were excised. All organs were washed with physiological saline and dried with filter paper for *ex vivo* imaging of DiD fluorescence through an *in vivo* imaging system (Quick View 3000, Bio-Real, Austria).

In order to study the difference of the distribution behavior of HA micelles in normal rats and hepatic fibrosis rats, hepatic fibrosis rats were randomly divided into three groups ($n = 5$) and the following steps were in agreement with the foregoing. To research the role of HA in distribution, we added HA-containing groups which HA solution (100 kDa, 10 mg/mL) was injected 15 min prior to administration of micelles and HA micelles.

In addition, in order to investigate the distribution of HA micelles in different liver cells, liver cells were isolated from normal liver and fibrotic liver at 15 min after intravenous injection of DiD solution, DiD micelles and DiD-HA micelles (DiD concentration was 10 μg/kg). Fluorescent intensity of cells was measured by flow cytometer to characterize the distribution of HA micelles.

2.13. Immunofluorescence staining

The distribution of HA micelles in liver tissues was researched by immunofluorescence staining. C6 solution, C6 micelles and C6-HA micelles (C6 concentration was 200 μg/kg) were injected intravenously to normal rats and hepatic fibrosis rats, respectively. After 15 min, rats were sacrificed and liver tissues were used to make frozen sections (8 μm) by a cryostat microtome (Leica, CM1960, Germany) kept at −40 °C. Sections were fixed with 4% paraformaldehyde for 5 min at 4 °C, washed with PBS for 3 min thrice, and incubated with 0.5% (*w/w*) Triton X-100 in PBS for 5 min at room temperature. Then, sections were washed two times

with PBS and blocked with 2% (*w*/*w*) bovine serum albumin (BSA) for 1 h at room temperature, followed by the incubation with primary antibody (CD44 affinity purified sheep IgG 1:100, diluted with PBS) overnight at 4 °C. Sections were washed three times with PBS (10 min each time) and incubated with second antibody (Alexa 557-labeled anti-mouse IgG 1:500, diluted with PBS) for 1 h at room temperature. Sections were washed three times with PBS and stained with DAPI for 5 min. After washing three times with PBS, antifade mounting medium was added to sections and the sections were mounted with cover slips. Finally, sections were viewed with CLSM.

2.14. *In vivo anti-hepatic fibrosis research*

Male SD rats were randomly divided into five groups ($n = 15$): normal group, physiological saline group, SLB solution group, SLB micelles group and SLB-HA micelles group. Normal group was not treated and the other four groups were induced liver fibrosis model by intraperitoneal injection of CCl_4 twice a week. After 4 weeks, these four groups were simultaneously injected with physiological saline, SLB solution, SLB micelles and SLB-HA micelles (SLB concentration was 5 mg/kg) twice a week, respectively. Rats were sacrificed ($n = 5$) and liver tissues were excised at 6, 7 and 8 weeks, respectively. Liver appearance and histological analysis (H&E stain and Masson stain) were used to evaluate the degree of liver fibrosis. Meanwhile, blood was collected for the determination of aspartate transaminase (AST) and alanine transaminase (ALT) levels, which are the important indicators for liver fibrosis.

The root cause of liver fibrosis is that the HSCs are activated and proliferated, so the number of activated HSCs and the total amount of HSCs can reflect the degree of liver fibrosis. The cytoplasm of HSCs contains desmin and activated HSCs can express smooth muscle actin (SMA). Therefore, desmin stain and SMA stain were used to further evaluate the therapeutic effect after 8 weeks of treatment.

According to research reports, long term repeated exposure to CCl_4 can lead to aplastic anemia[56]. Drugs in the treatment process of liver fibrosis induced by CCl_4 may improve the side effects of bone marrow suppression. In order to verify our conjecture, we examined the blood routine index of each group at 6, 7 and 8 weeks, respectively. Briefly, 0.3 mL of blood was collected in Eppendorf tubes (containing EDTA-2K$^+$), then white blood cells (WBCs), red blood cells (RBCs) and platelets (Plts) were counted by automated hematology analyzer (MEK-6318K, Nijon-kohden, Shinjuku-ku, Japan) as indices of bone marrow suppression[57].

2.15. *Safety evaluation*

Male SD rats were randomly divided into two groups ($n = 5$). Physiological saline and blank HA micelles (concentration was 50 mg/kg) were administered intravenously once every other day. After 4 weeks, the rats were sacrificed. Blood and serum were collected for routine analysis and biochemical index detection, respectively. Major organs were excised and processed for histological analysis (H&E stain) to evaluate the systemic organ toxicity of HA micelles.

In addition, the excessive use of sodium deoxycholate may produce hemolysis, so we carried out a study on the hemolysis of HA micelles[58]. Briefly, 5 mL of fresh rabbit blood was diluted with 10 mL physiological saline. RBCs were isolated from serum by centrifugation after the removal of fibrinogen. Next, RBCs were washed three times and diluted to 2% RBCs suspension by physiological saline for subsequent experiments. Then, 0.5 mL of RBCs suspension was added to 0.5 mL of HA micelles at varied concentrations (0.078, 0.156, 0.3125, 0.625, 1.25, 2.5, 5, and 10 g/L). All samples were mixed and incubated for 4 h at 37 °C. Triton X-100 (10 g/L) and PBS were used as positive and negative controls, respectively. Samples were centrifuged (3000 rpm, 10 min) and 100 μL of supernatant was transferred to a 96-well plate to measure the hemolysis with a microplate reader (Thermo Scientific Varioskan Flash, Thermo Fisher Scientific, USA) at 540 nm. The hemolysis ratio was calculated according to Eq. (4)[59]:

$$\text{Hemolysis ratio} = (A_{\text{sample}} - A_{-})/(A_{+} - A_{-}) \times 100\% \quad (4)$$

where A_{sample}, A_{-} and A_{+} represent the optical density of samples, negative and positive controls, respectively.

2.16. *Statistics*

Results represent mean±standard deviations (SD). Student's *t*-test was performed for comparison between two groups. A value of P less than 0.05 was considered statistically significant and a value of P less than 0.01 was considered highly significant.

3. Results and discussion

3.1. *Synthesis of optimal HA−DOCA conjugate*

In order to prepare the amphiphilic HA−DOCA conjugate, ethylenediamine was used to link hydrophobic deoxycholic acid to hydrophilic HA. Partial carboxyl groups of HA were modified with deoxycholic acid and the hydrophilic HA was changed to amphiphile. The chemical structure of HA−DOCA was confirmed by ^{1}H NMR (Fig. 2). The characteristic peaks of HA appeared at 2.00 ppm (−$COCH_3$−) and 3.30−4.80 ppm (sugar ring). As for HA−DOCA, the additional characteristic peaks of DOCA (0.20−1.50 ppm) indicated the successful synthesis of HA−DOCA. The amount of deoxycholic acid in HA−DOCA was quantitatively characterized using the integration ratio between the characteristic peaks of the *N*-acetyl group in HA (2.00 ppm, 3H, −$COCH_3$−) and the methyl group in deoxycholic acid (0.80 ppm, 3H, −CH_3). The molecular weight of HA was about 100 kDa and the substituting degree of HA−DOCA was about 9.4% which has the best liver targeting effect (Supporting Information Fig. S1).

3.2. *Characterization of micelles and HA micelles*

Micelles and HA micelles were prepared by thin film hydration method. The final prescription has been optimized (Supporting Information Tables S1 and S2 and Fig. S2). As shown in Table 1, the particle size of micelles and HA micelles was about 40 nm, which was consistent with the result observed in TEM (Fig. 3). HA micelles showed a larger particle size and negative zeta potential, which was due to the surfaces of micelles were wrapped by HA. TEM images showed that the micelles and HA micelles were almost spherical in shape. Such small particle size guaranteed HA micelles to avoid being cleared by liver reticuloendothelial system (RES), pass through small holes in LSECs and then reach HSCs site successfully. The negative zeta potential could protect HA micelles from being neutralized by cationic proteins in plasma. Small amount of vesicle structure presented in

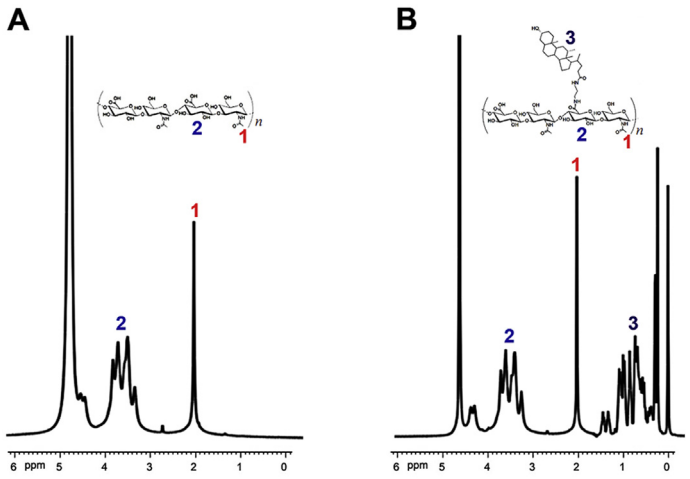

Figure 2 ^{1}H NMR spectra of (A) HA and (B) HA−DOCA conjugate.

the two TEM images, probably because small amount of phospholipid didn't form micelles with sodium deoxycholate, but spontaneously formed vesicles.

The CMC values of micelles and HA micelles were determined by fluorescence spectrophotometer using pyrene as a probe. Micelles and HA micelles had the similar CMC value. Such low CMC value guaranteed HA micelles to maintain their original shape under the highly diluted conditions of blood before reaching HSCs site. Based on above results, HA micelles have great potential to be HSCs targeting drug carriers.

The *in vitro* stability of micelles and HA micelles were evaluated in PBS (pH 7.4) and serum. Compared with the original size, the particle size of micelles and HA micelles increased approximately 10 nm in PBS and the particle size increased approximately 20 nm in serum after 24 h (Fig. 3E). There was no significant change in the size of micelles and HA micelles. These results proved the excellent stability of micelles and HA micelles in PBS and serum.

3.3. *Characterization of SLB micelles and SLB-HA micelles*

Using thin film hydration method, hydrophobic SLB was easily encapsulated into micelles. The characteristics of SLB micelles and SLB-HA micelles, including particle size, poly dispersive index (PDI), CMC value, DL and EE, were shown in Table 2. There were no significant changes in particle size and CMC value after drug loading. The EE of SLB micelles and SLB-HA micelles was consistently above 90%, illustrating that SLB was well incorporated into micelles.

Table 1 Characterization of micelles and HA micelles.

Entry	Particle size (nm)	PDI	Zeta potential (mV)	CMC (mg/L)
Micelles	39.8±1.3	0.197±0.02	−8.3±1.2	20.7
HA micelles	44.9±2.1	0.154±0.01	−15.2±2.3	21.1

HA, hyaluronic acid; PDI, poly dispersive index; CMC, critical micelle concentration.
Data represent mean ± SD (n = 3).

3.4. *HA micelles have an excellent in vivo sustained release effect*

Fig. 3F shows the *in vitro* release of SLB solution, SLB micelles and SLB-HA micelles. Slow release of SLB from micelles was observed. For example, about 90% cumulative release was observed for SLB solution, while about 60% cumulative release was achieved by SLB micelles and 40% by SLB-HA micelles after 24 h. The release rate of SLB from micelles was significantly lower than SLB solution, and the cumulative release of SLB from SLB-HA micelles was lower than SLB micelles. This indicated that HA micelles had a good sustained release effect *in vitro*.

3.5. *HA micelles can be selectively uptaken by HSCs in vitro*

In order to research the cellular internalization of micelles, we used DiD as fluorescent marker and prepared DiD-loaded micelles (DiD micelles) and DiD-loaded HA micelles (DiD-HA micelles). HSCs ($CD44^{+}$), HepG2 ($CD44^{+}$), LO2 ($CD44^{-}$) and RAW 264.7 ($CD44^{-}$) were selected as experimental cells. From Fig. 4A (group a), fluorescence intensity of HSCs incubated with DiD-HA micelles was approximately 5-fold and 2-fold higher than these incubated with DiD solution and DiD micelles, respectively. When HSCs were simultaneously incubated with HA solution (group b), the cell uptake efficiency of DiD-HA micelles was reduced substantially, however the cell uptake efficiency of DiD solution and DiD micelles was not affected. Results were similar in HepG2 cells. The differences between HA-absent systems and HA-containing systems could be explained by the fact that free HA could compete the binding sites on the CD44 receptors thus resulting in the decreased cellular uptake of DiD-HA micelles. In LO2 cells, DiD micelles and DiD-HA micelles showed no significant differences in cellular uptake efficiency. These results further demonstrated that HA micelles can specifically bind to CD44 and internalize into $CD44^{+}$ cells *via* CD44 receptor-mediated endocytosis. The uptake efficiency of DiD micelles by RAW cells was significantly higher than that of DiD-HA micelles. This was because DiD micelles with a certain particle size were removed by RAW cells as foreign matter. However, the surface of DiD-HA micelles coated with hydrophilic HA could form a thick hydration layer on the surface of micelles after absorbing water, causing HA

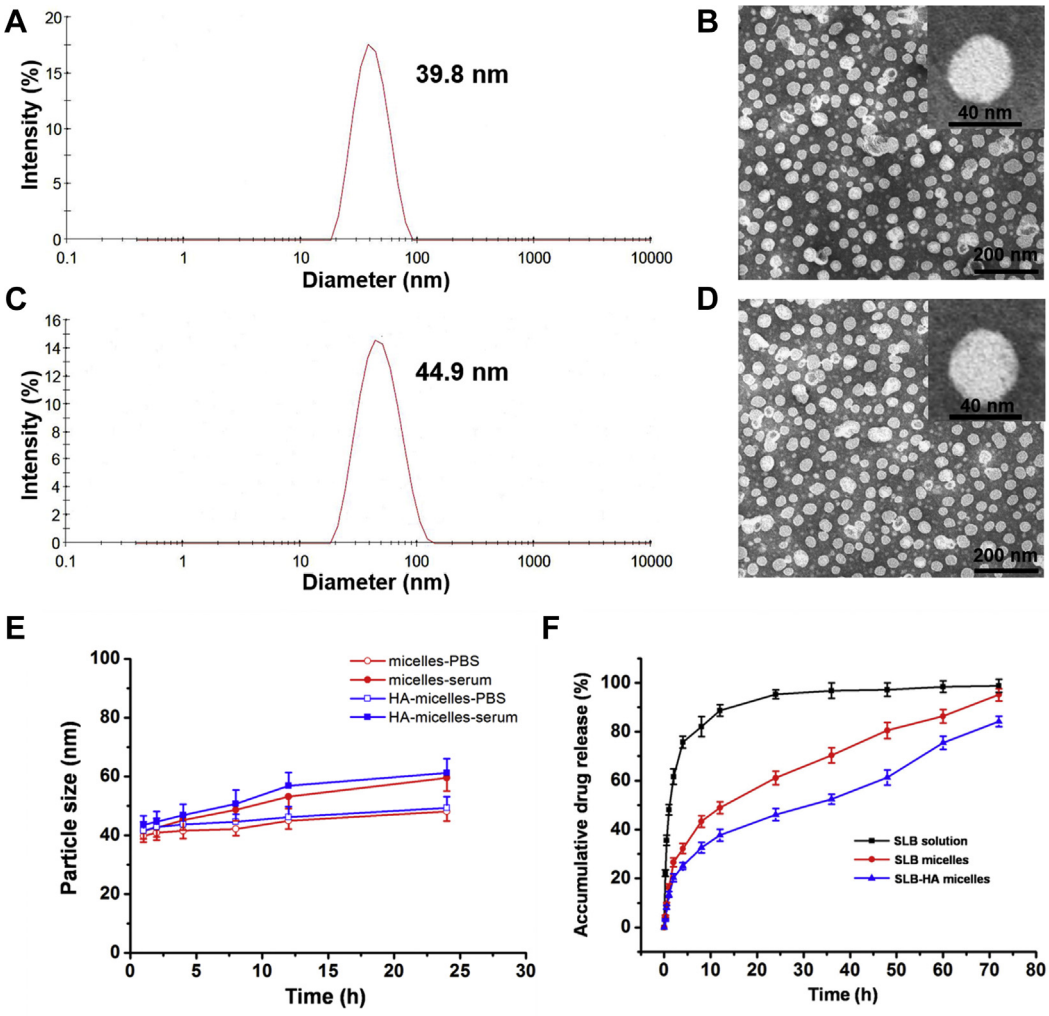

Figure 3 Size distribution and morphology of micelles: DLS size measurement of (A) micelles and (C) HA micelles; TEM image of (B) micelles and (D) HA micelles. (E) The stability of micelles and HA micelles in serum and PBS (pH 7.4) for 24 h. Data represent mean ± SD ($n = 3$). (F) SLB release profiles of SLB solution, SLB micelles and SLB-HA micelles in PBS at pH 7.4. Data represent mean ± SD ($n = 3$).

micelles to be mistaken for water and avoid being swallowed by RAW cells. Therefore, HA micelles could be selectively uptaken by HSCs, while avoiding their distribution in normal hepatocytes and the phagocytosis of macrophages. HA micelles have the potential of HSCs targeting. In addition, the cellular uptake results of HepG2 cells indicated that HA micelles could also be used as carriers for liver cancer targeted therapy.

CLSM was used to investigate the intracellular distribution profile of HA micelles. As shown in Fig. 4B, red fluorescence representing DiD was obviously observed in the cell nuclei periphery of HSCs and HepG2 cells after 4 h incubation with DiD-HA micelles. This became the direct visual evidence of the cell internalization of HA micelles and the release of the loaded DiD. HSCs and HepG2 cells treated with DiD-HA micelles showed the obviously increased nuclear and perinuclear fluorescence intensity compared with DiD solution and DiD micelles. However, for LO2 cells, there were no significant differences in cellular uptake efficiency. This further proved the critical role of HA in mediating HA micelles internalization in HSCs *via* CD44 receptors. Meanwhile, CLSM results intuitively proved that HA micelles could effectively avoid being cleared by macrophages.

Table 2 Characterization of SLB micelles and SLB-HA micelles.

Entry	Particle size (nm)	PDI	CMC (mg/L)	DL (%)	EE (%)
SLB micelles	41.2±1.5	0.186±0.02	20.5	6.9±0.3	91.1±1.1
SLB-HA micelles	45.4±2.3	0.179±0.03	20.8	6.2±0.2	92.2±1.4

SLB micelles, SLB loaded micelles; SLB-HA micelles, SLB loaded HA micelles; DL, drug loading capacity; EE, entrapment efficiency. Data represent mean ± SD ($n = 3$).

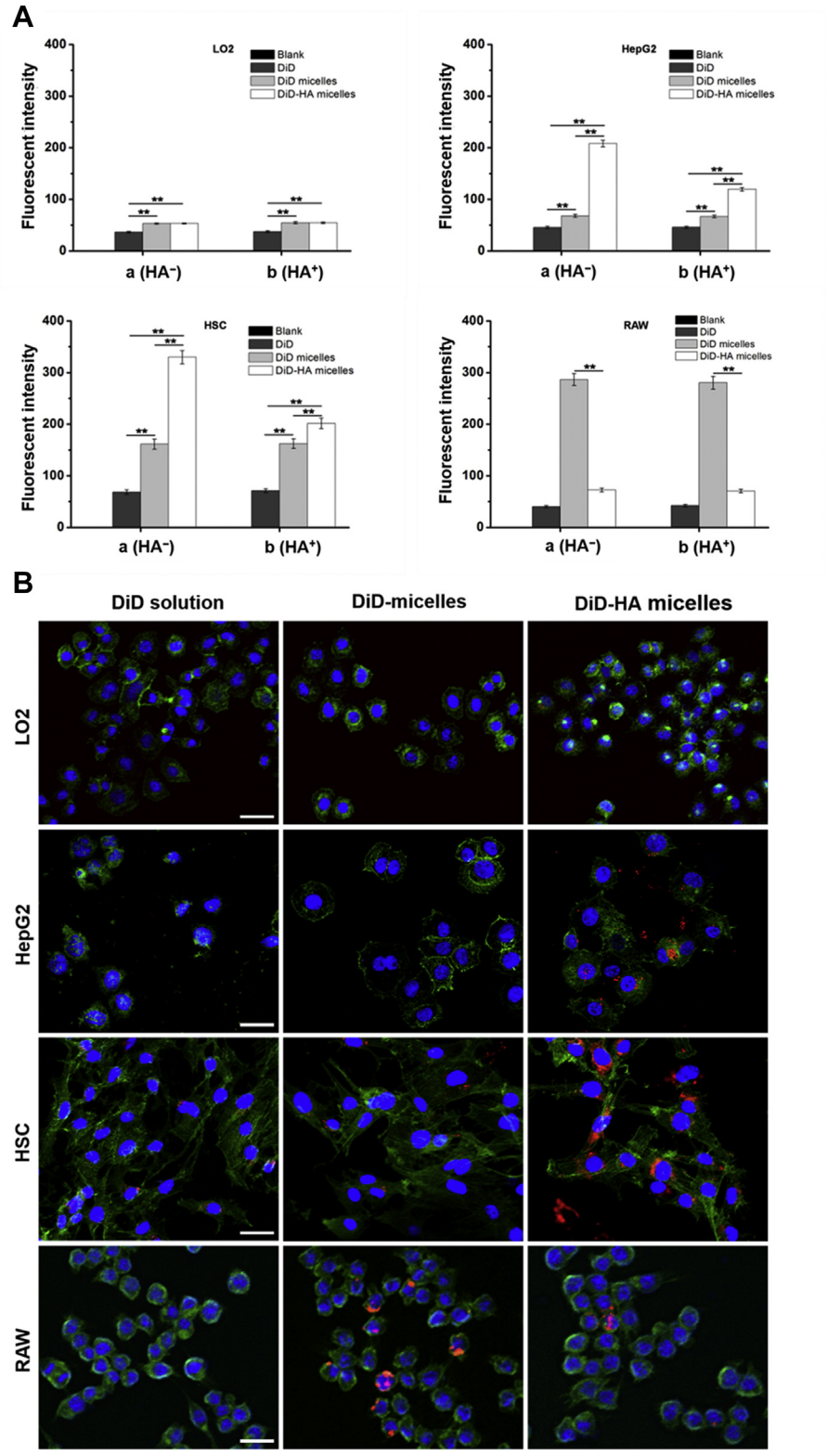

Figure 4 (A) Cellular uptake of DiD solution, DiD micelles and DiD-HA micelles after incubation with LO2, HepG2, HSCs and RAW cells for 4 h, observed by flow cytometric analysis. Group a (HA^-): cells were incubated with preparations solely; Group b (HA^+): cells were simultaneously incubated with HA solution (10 mg/mL, 100 kDa) and preparations. Data represent mean ± SD ($n = 3$). $^{*}P < 0.05$; $^{**}P < 0.01$. (B) CLSM images of LO2, HepG2, HSCs and RAW cells incubated with DiD solution, DiD micelles and DiD-HA micelles for 4 h. The cell nuclei were stained with DAPI (blue), cell membranes were stained with FITC-labeled phalloidin (green) and DiD fluorescence displayed in red. The scale bar represents 100 μm.

3.6. *Successful construction of liver fibrosis rat model*

Liver fibrosis rat model was induced by intraperitoneal injection of CCl_4 dissolved in soybean oil (2:3, *v/v*) for 8 weeks. Fig. 5A shows the differences between fibrotic liver and normal liver. Normal liver had bright red color, luster, soft texture, smooth and delicate surface. However, fibrotic liver was swollen, the color changed to dark red, the liver lost its luster and the surface was rough. More differences were confirmed clearly by H&E stain and Masson stain. The sections of normal liver showed a negligible amount of collagen and ECM, whereas the fibrotic liver showed an obvious increase in ECM with collagen bundles surrounding the

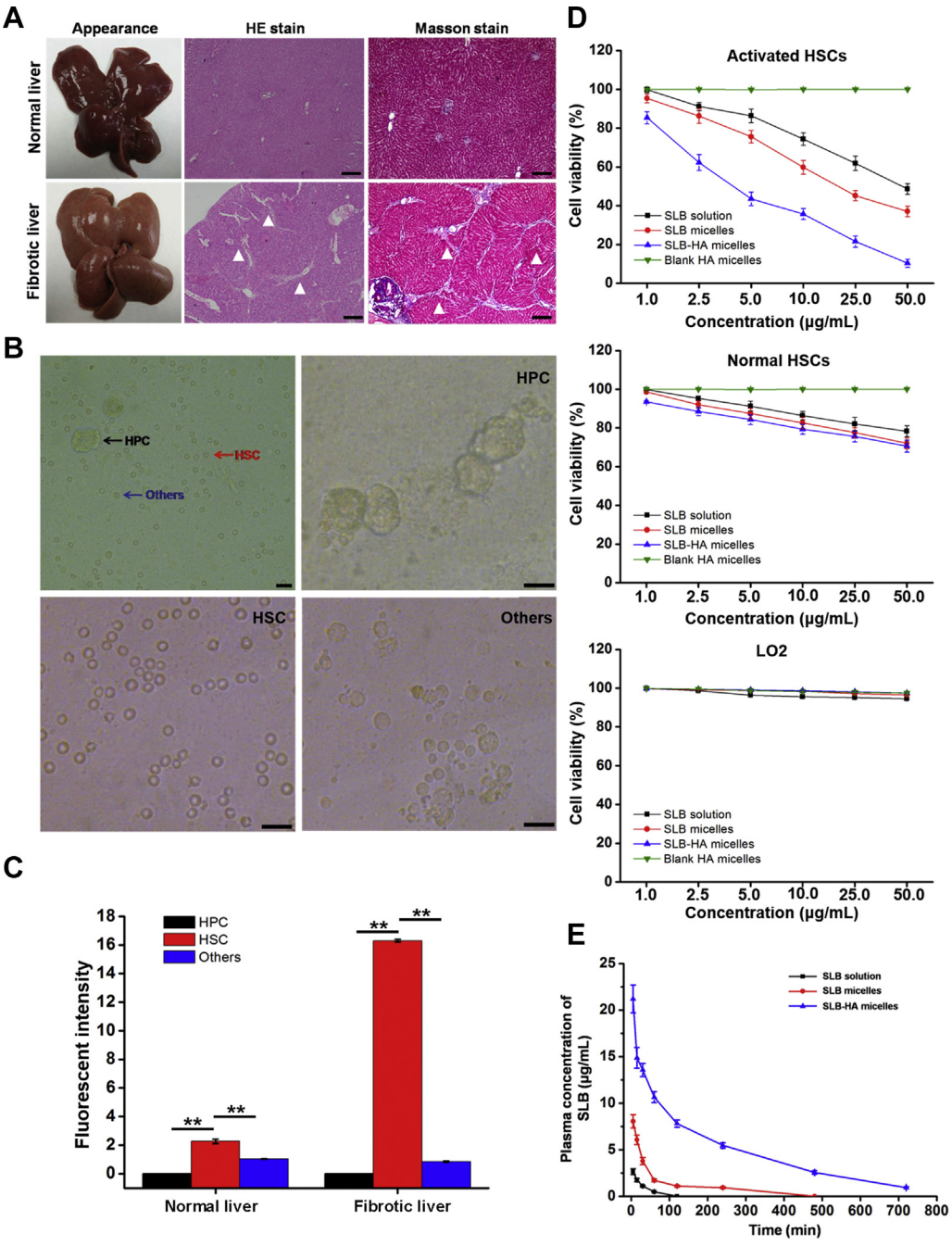

Figure 5 (A) Appearance and histological images of normal and fibrotic livers after H&E stain and Masson stain. Arrowheads indicate collagen fibrils. The scale bar represents 200 μm. (B) Isolated HPCs, HSCs and other non-parenchymal cells. The scale bar represents 100 μm. (C) The expression of CD44 receptor in HPCs, HSCs and other non-parenchymal cells, observed by flow cytometric analysis. Data represent mean ± SD ($n = 3$). $^{*}P < 0.05$; $^{**}P < 0.01$. (D) *In vitro* cell viability of SLB solution, SLB micelles, SLB-HA micelles and blank HA micelles against activated HSCs, normal HSCs and LO2 cells. Data represent mean ± SD ($n = 3$). (E) *In vivo* pharmacokinetic profiles after intravenous injection of SLB solution, SLB micelles and SLB-HA micelles in rats. Data represent mean ± SD ($n = 5$).

liver lobules. In addition, the body weight of model rats kept lower than that of normal rats in the whole process of modeling, which indicated the occurrence of disease (Supporting Information Fig. S3).

3.7. *Successful separation of HPCs, HSCs and other non-parenchymal cells*

Liver is mainly composed of HPCs, HSCs and other non-parenchymal cells. At present, the common method of liver cell isolation is portal vein catheterization perfusion technique[53]. Fig. 5B shows the cells after perfusion and these three kinds of cells can be observed clearly. After the first centrifugation (600 rpm for 8 min), the largest HPCs were centrifuged to the bottom of the tube. Compared with other non-parenchymal cells, the density of HSCs is slightly smaller[53]. The HSCs were existed in the supernatant after the second centrifugation (2000 rpm for 10 min) and the sediments were other non-parenchymal cells. Newly isolated HSCs were round, bright and had clear boundary. Because HSCs were rich in lipid droplets, their transmittance was significantly stronger than other cells. In summary, we have successfully separated these three kinds of cells for follow-up research.

3.8. *HSCs have high and specific CD44 expression in fibrotic liver*

In liver, the specificity of CD44 receptors expressed in HSCs can ensure the therapeutic effect of drug loaded HA micelles and reduce their toxic side effects on other liver cells. Therefore, it is very important to determine the expression of CD44 in different liver cells. FITC-labeled CD44 antibody was used to measure CD44 expression. As shown in Fig. 5C, CD44 was not expressed on the surface of HPCs. In normal liver, other non-parenchymal cells expressed only tiny amounts of CD44 which may be due to the presence of Kupffer cells[60,61]. The number of CD44 in HSCs was about two times of that in other non-parenchymal cells. In fibrotic liver, there was no significant change in the expression of CD44 in other non-parenchymal cells. However, the expression

Table 3 Pharmacokinetic parameters of SLB, SLB micelles and SLB-HA micelles.

Sample	SLB	SLB micelle	SLB-HA micelle
Dose (mg/kg)	10.0	10.0	10.0
C_{max} (μg/mL)[a]	2.64 ± 0.3	8.04 ± 0.7*	21.2 ± 1.5$^{*\&}$
T_{max} (min)[b]	5	5	5
AUC (h·μg/L)[c]	3.11	11.72*	97.52$^{*\&}$
AUC/dose (h·kg/L)	3.11×10^{-4}	$1.172 \times 10^{-3*}$	$9.752 \times 10^{-3*\&}$
$t_{1/2}$ (min)	20.1	25.6*	104.3$^{*\&}$

AUC, area under the curve. All values are mean ± SD ($n = 5$).
$^{*}P < 0.01$ *vs.* SLB; $^{\&}P < 0.01$ *vs.* SLB micelles.

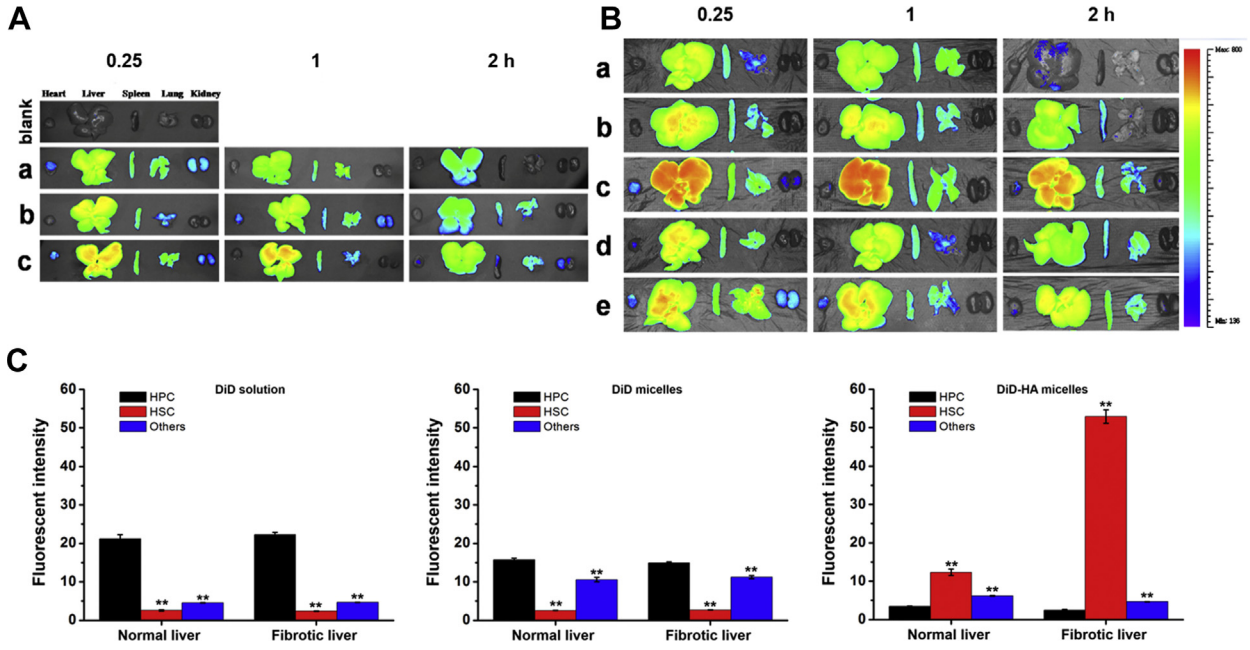

Figure 6 (A) *Ex vivo* DiD fluorescence images showing the bio-distribution of (a) DiD solution, (b) DiD micelles and (c) DiD-HA micelles in normal rats at 0.25, 1 and 2 h post-injection. (B) *Ex vivo* DiD fluorescence images showing the bio-distribution of (a) DiD solution, (b) DiD micelles, (c) DiD-HA micelles, (d) HA + DiD micelles and (e) HA + DiD-HA micelles in liver fibrosis rats at 0.25, 1 and 2 h post-injection. (C) Quantitative analysis of the hepatocellular distribution of DiD solution, DiD micelles and DiD-HA micelles in normal and liver fibrosis rats. Data represent mean ± SD ($n = 3$). $^{**}P < 0.01$ *vs.* HPC.

of CD44 in HSCs had a significant increase which was about 8-fold of that in normal liver. These results indicated that HSCs were the main cells of CD44 expression in the liver and the CD44 expression of HSCs increased significantly after the occurrence of hepatic fibrosis. The specificity of CD44 expression in the liver was advantageous to the specific targeting of HA micelles.

3.9. SLB-HA micelles can selectively promote the apoptosis of activated HSCs in vitro

The root cause of liver fibrosis is the activation and proliferation of HSCs. Therefore, reversing the activation of HSCs and decreasing the number of activated HSCs is the most fundamental way to treat liver fibrosis. In activated HSCs, SLB-HA micelles revealed a significantly higher cytotoxicity compared with SLB solution and SLB micelles at the equivalent drug concentration, whereas the cytotoxicity of SLB-HA micelles was significantly reduced in normal HSCs (Fig. 5D). Moreover, SLB-HA micelles didn't show significant toxicity to normal liver cells (LO2 cells). Thus, SLB-HA micelles could selectively promote the apoptosis of activated HSCs without causing significant toxicity to other normal cells in the liver, which facilitated the treatment of liver fibrosis and reduced the side effects of the formulation.

3.10. HA micelles have a good long circulation effect in vivo

Micelles could be diluted as soon as they enter the blood circulation after intravenous administration. Most of micelles were distributed to different organs, leaving small amounts of micelles

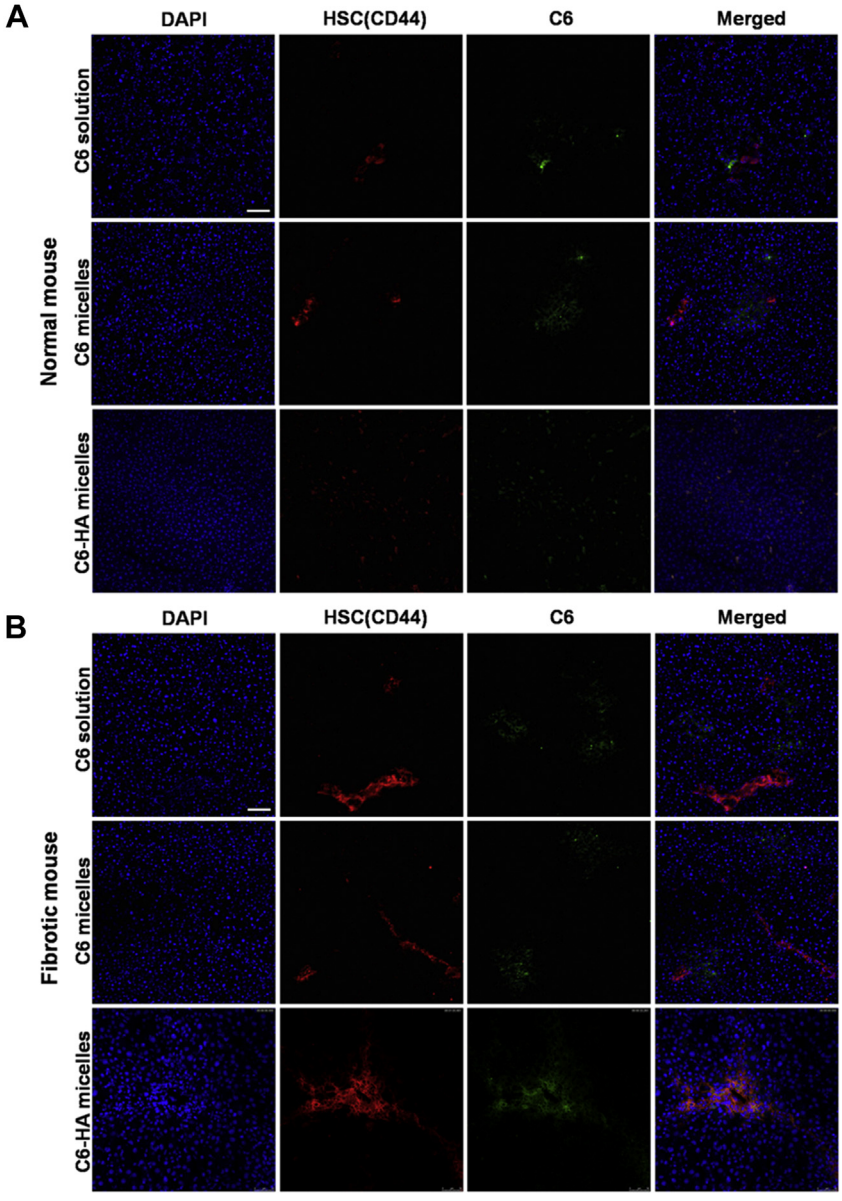

Figure 7 The immunolocalization of C6 solution, C6 micelles and C6-HA micelles in (A) normal and (B) liver fibrosis rats. The cell nuclei were stained with DAPI (blue), CD44 receptors (HSCs) were stained with Alexa 557-labeled anti-mouse IgG (red) and C6 fluorescence displayed in green. The scale bar represents 200 μm.

in the blood[62–64]. Therefore, it is very important to prolong blood circulation and retard blood clearance of micelles in order to increase the distribution to HSCs site. Fig. 5E and Table 3 show the pharmacokinetic result. The release of SLB from SLB-HA micelles continued for 12 h, whereas the serum drug concentration of SLB solution group and SLB micelles group dropped to baseline level within 2 and 8 h, respectively. Compared with SLB solution and SLB micelles, the blood circulation time of SLB-HA micelles was greatly extended. The area under the curve of SLB-HA micelles was 30.4-fold and 7.3-fold higher than that of SLB solution and SLB micelles, respectively. The similar results were observed between *in vitro* and *in vivo* tests. These results indicated that HA micelles had a good long circulation effect *in vivo*, which might be because HA could act as a protective coating and then reduce the clearance of micelles from the blood.

3.11. HA micelles have a significant HSCs targeting effect in hepatic fibrosis rats

Then we studied the difference of the distribution behavior of HA micelles in normal rats and hepatic fibrosis rats. Fig. 6A shows the fluorescent images of major organs after administration in normal rats. For DiD solution group, liver, spleen and lung showed strong fluorescence, indicating that DiD was mainly captured and metabolized by these organs. Compared with DiD solution, the increased accumulation in liver for DiD micelles could be observed which might be attributed to the phagocytosis of RES. The accumulation in liver of DiD-HA micelles was further increased compared to DiD micelles, which was due to the CD44 receptor-mediated endocytosis. In fibrotic liver, there were no significant differences in the distribution behavior of DiD solution and DiD micelles compared to normal liver (Fig. 6B). However, the increase of DiD-HA micelles in liver was very obvious, which was attributed to the dramatic increase in the expression of CD44 when liver fibrosis occurred. These results were consistent with the experimental results of CD44 expression. Further research showed that, there was no obvious change in the distribution behavior of DiD micelles when HA solution was injected in advance. However, the distribution of DiD-HA micelles in liver was significantly decreased. This may be because HA solution pre-saturated CD44 receptors in the liver, resulting in the decrease in targeting efficiency of HA micelles. These results indicated that HA micelles could specifically target to the liver through CD44. The CD44 expression of liver increased significantly after the

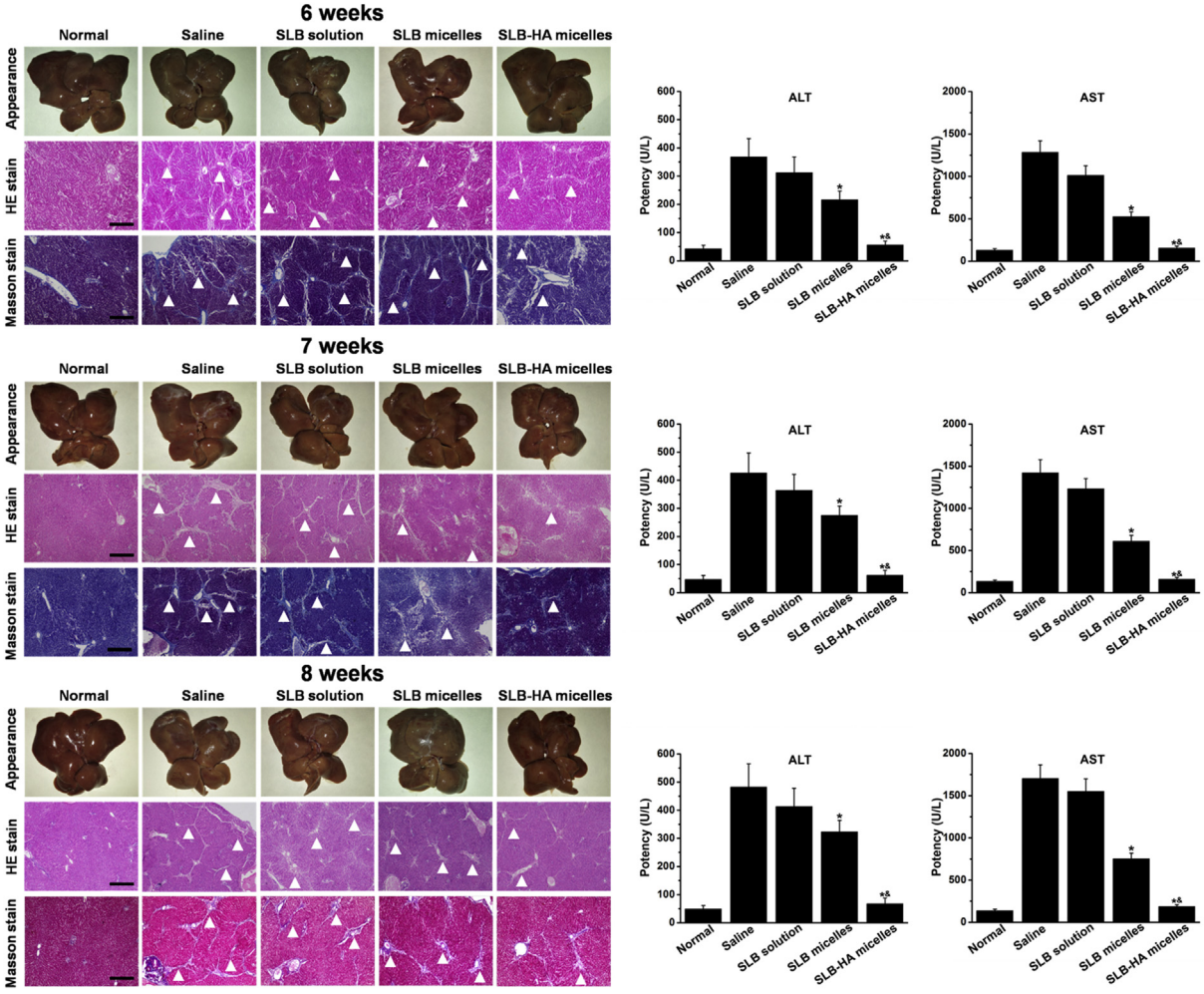

Figure 8 Representative photos of liver appearance, H&E and Masson stained liver sections obtained from normal rats and fibrotic rats treated with physiological saline, SLB solution, SLB micelles and SLB-HA micelles at 6, 7 and 8 weeks, respectively. AST and ALT levels of each group were detected simultaneously. Arrowheads indicate collagen fibrils. The scale bar represents 200 μm. Data represent mean ± SD ($n = 5$). $^{*}P < 0.01$ *vs.* SLB solution; $^{\&}P < 0.01$ *vs.* SLB micelles.

occurrence of fibrosis meanwhile the liver targeting ability of HA micelles was also improved.

The distribution of DiD solution, DiD micelles and DiD-HA micelles in different liver cells was quantified by flow cytometer. As shown in Fig. 6C, the distribution of DiD solution was mostly in HPCs which might be because the number of HPCs accounted for more than 60% in the liver. When liver fibrosis occurred, the number of HPCs wouldn't have significant change resulting in the constant distribution of DiD solution in hepatic fibrosis rats. The distribution of DiD micelles in other non-parenchymal cells was significantly increased in normal liver and fibrotic liver, which might be due to the phagocytosis of other non-parenchymal cells such as Kupffer cells. In contrast, DiD-HA micelles were mainly accumulated in HSCs which was attributed to a combination between HA and CD44 receptors resulting in an increase in cellular uptake by HSCs. Because of the increase in HSCs number and CD44 expression after the occurrence of fibrosis in the liver, the distribution of DiD-HA micelles in HSCs was significantly increased compared to normal liver (about 5-fold).

3.12. Immunofluorescence staining of liver sections in normal and liver fibrosis rat model

To investigate the distribution of HA micelles in normal and fibrotic liver tissues, Alexa 557 (red fluorescence) was used to label HSCs which was in coincided with the red fluorescence of DiD. So we replaced DiD with C6 (green fluorescence) to label micelles. As shown in Fig. 7, the fluorescence of C6-HA micelles and CD44 receptors was overlapped each other reflecting the targeting effect of HA micelles to HSCs in both normal and fibrotic livers. However, C6 solution and C6 micelles were distributed to other liver cells in addition to HSCs. This once again proved that HA micelles had an obvious HSCs targeting effect and were rarely distributed to other liver cells. They had great potential as HSCs targeting drug carriers to treat liver fibrosis. In addition, we can also see that the expression of CD44 in fibrotic liver was much higher than that of normal liver, which indicated the proliferation of HSCs accompanied by the increase of CD44 in fibrotic liver.

3.13. SLB-HA micelles have an excellent anti-hepatic fibrosis effect in vivo

Hepatic fibrosis rats were treated with various preparations after 4 weeks of modeling. As shown in Fig. 8, obvious white stripe appeared on the liver surface indicated severe disease in the liver. H&E stain and Masson stain results showed that the liver of saline group had a large amount of collagen and ECM which proved the occurrence of serious fibrosis. For three SLB treatment group, the degree of fibrosis was significantly reduced which reflected the definite therapeutic effect of SLB on hepatic fibrosis. The liver treated with SLB-HA micelles showed a

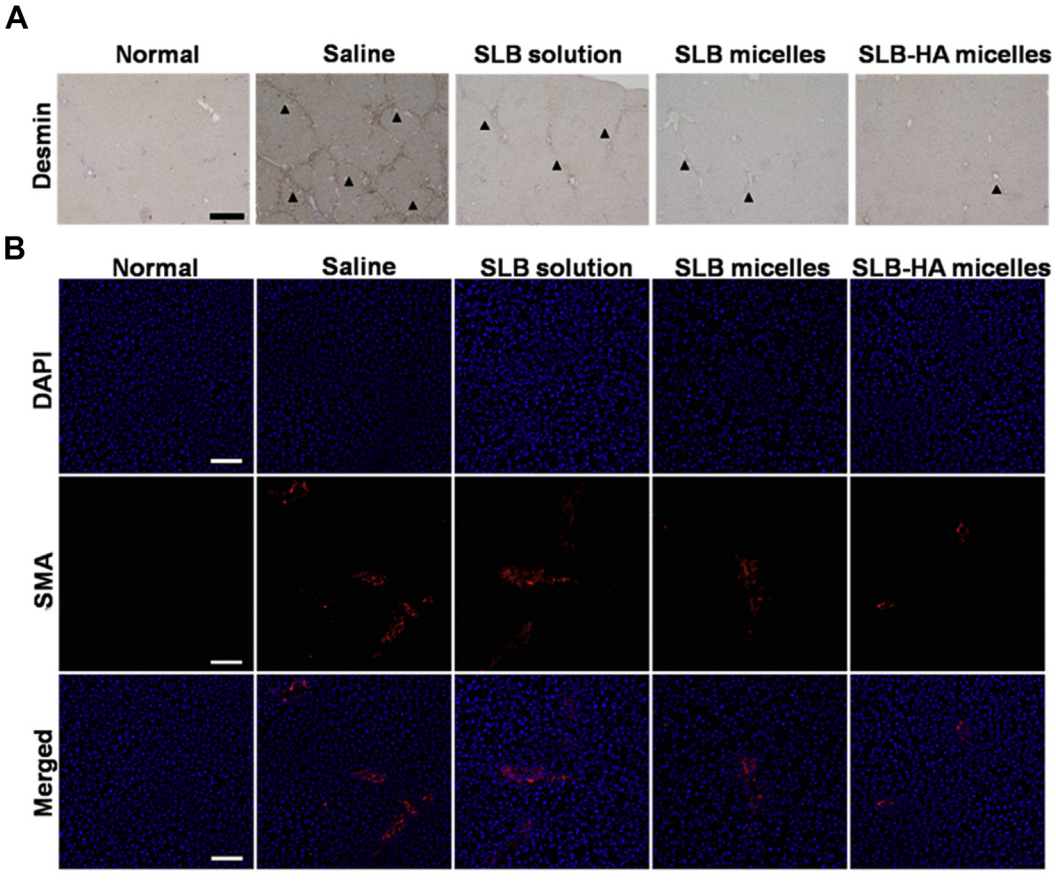

Figure 9 (A) Desmin stain of each group at 8 weeks. Arrowheads indicate desmin (HSCs). The scale bar represents 200 μm. (B) SMA stain of each group at 8 weeks. The cell nuclei were stained with DAPI (blue) and the SMA (activated HSCs) were stained with Cy3-labeled anti-mouse IgG (red). The scale bar represents 200 μm.

smooth and bright surface, which was no different from the normal liver. Section staining results showed that the liver of SLB-HA micelles treated group had a very small amount of collagen and ECM compared with other groups, which indicated the excellent anti-hepatic fibrosis effect of SLB-HA micelles. With the increase of treatment time, livers of SLB solution and SLB micelles groups showed a tendency to become better, but the liver fibrosis was still serious. However, the degree of hepatic fibrosis in SLB-HA micelles group was always at a low level. This finding was remarkable. The occurrence of liver fibrosis can cause many physiological changes in the body. Among them, ALT and AST levels are representative indices to judge the degree of fibrosis. Comparing with normal rats, ALT and AST levels of hepatic fibrosis rats were significantly increased and continued to increase with the exacerbation of fibrosis. However, ALT and AST levels of SLB-HA micelles group were always low which were closed to normal level. In addition, the body weight of the rats treated with SLB-HA micelles increased significantly and was close to that of normal rats, which indicated that SLB-HA micelles could significantly improve the living conditions of fibrotic rats (Supporting Information Fig. S4). Therefore, SLB-HA micelles had good therapeutic potential for hepatic fibrosis.

As said in the Section Introduction, when hepatic fibrosis occurred, the number of HSCs increased significantly. The cytoplasm of HSCs contains a large number of desmin, so the expression of desmin can reflect the degree of fibrosis. As shown in Fig. 9A, the desmin expression of SLB-HA micelles group was significantly lower than other groups. Therefore, SLB-HA micelles could prevent the proliferation of HSCs and further play the role of anti-fibrosis.

The occurrence of hepatic fibrosis is essentially due to the change of HSCs from static state to active state. Therefore, reversing the activation of HSCs and reducing the number of activated HSCs is an important means for the treatment of liver fibrosis. Activated HSCs could express SMA specifically whereas quiescent HSCs don't express it. Then the expression of SMA can reflect the number of activated HSCs. As shown in Fig. 9B, the SMA expression level of SLB-HA micelles group was the lowest compared with other groups, which proved the least number of activated HSCs. Therefore, SLB-HA micelles could reverse the activation of HSCs and significantly improve liver fibrosis.

In addition, the blood test results showed that, SLB could improve the bone marrow suppression caused by repeated injection of CCl_4. SLB-HA micelles were more obvious to reduce this side effect (Fig. 10A).

3.14. *HA micelles have high safety*

As a drug delivery carrier, it is not only able to deliver drugs to the target site effectively, but also should have good safety itself. Blood routine analysis and biochemical index detection demonstrated the high safety of HA micelles to the body (Supporting Information Table S3). H&E stain proved that HA micelles had no obvious toxicity to major organs (Fig. 10B).

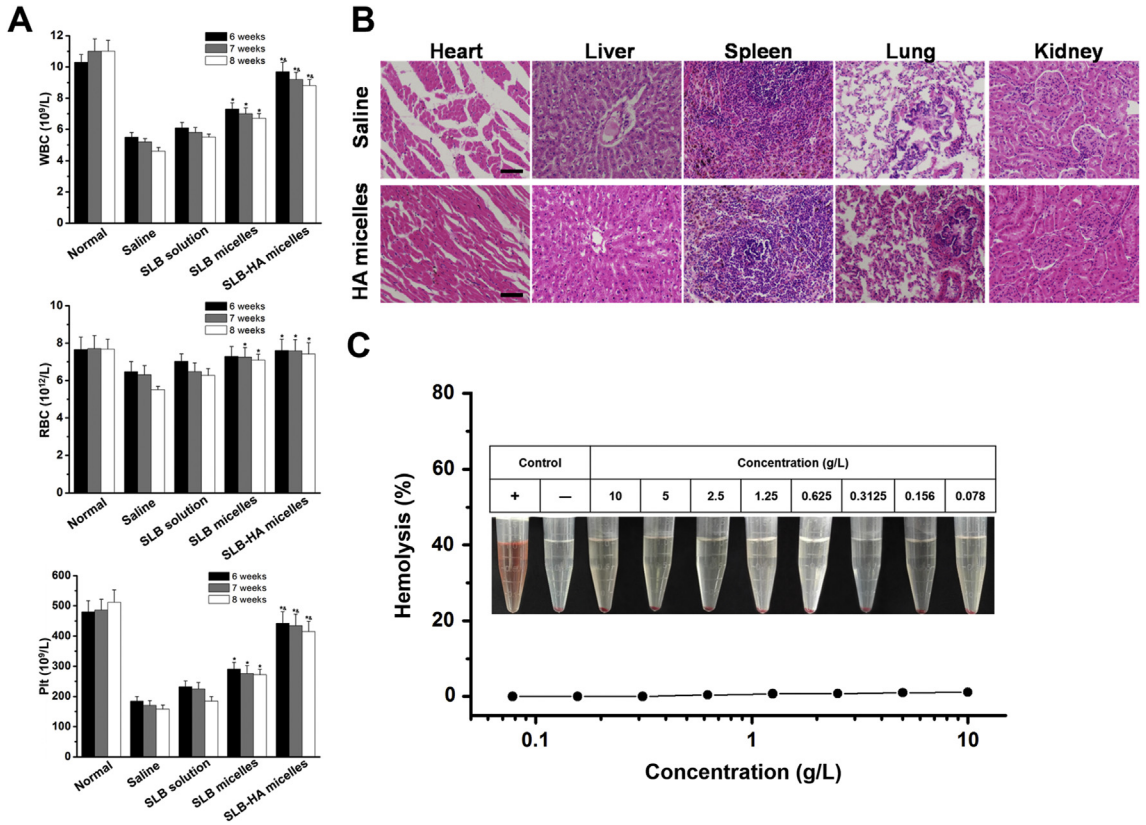

Figure 10 (A) WBC, RBC and Plt counts of normal rats and fibrotic rats treated with physiological saline, SLB solution, SLB micelles and SLB-HA micelles at 6, 7 and 8 weeks, respectively. Data represent mean ± SD ($n = 5$). $^{*}P < 0.01$ *vs.* SLB solution; $^{\&}P < 0.01$ *vs.* SLB micelles. (B) Histological observation (H&E stain) of major organs treated with physiological saline and HA micelles. The scale bar represents 200 μm. (C) Hemolytic activity of HA micelles.

The excessive use of sodium deoxycholate may produce hemolysis[58], so it was necessary to research the hemolysis of HA micelles. As shown in Fig. 10C, HA micelles showed the negligible hemolysis to RBCs even at the high concentration (10 g/L) which proved the excellent blood compatibility of HA micelles. In a word, HA micelles were very safe as drug delivery carriers.

4. Conclusions

In this study, we successfully synthesized HA−DOCA conjugate by using ethylenediamine as the linking group in order to increase the hydrophobicity of HA. Next, HA−DOCA conjugate was prepared as HA micelles combined with phospholipid and sodium deoxycholate as potential HSCs targeting carriers. HA micelles showed very small particle size which can guarantee them to pass through small holes in LSECs and reach HSCs successfully. SLB-HA micelles showed a good sustained release effect *in vitro* and long circulation effect *in vivo*. Moreover, HA micelles displayed specific uptake to HSCs *via* CD44 receptor-mediated endocytosis. Importantly, HA micelles showed significant liver targeting effect and that was more obvious in fibrotic liver which expressed more CD44 receptors. Flow cytometric detection and immunofluorescence staining results indicated that HA micelles could specifically target to HSCs rather than the other liver cells. *In vivo* anti-hepatic fibrosis research suggested the therapeutic ability of HA micelles for inhibiting and reversing the development of hepatic fibrosis. Safety investigation showed that HA micelles had excellent biological safety and biocompatibility. In summary, HA micelles represented a novel nanomicelles system which showed great potentiality in hydrophobic anti-hepatic fibrosis drugs delivery. In addition, HA micelles could be used for targeted therapy of liver cancers simultaneously, which also highly expressed CD44 receptors.

Acknowledgments

The work was financially supported by National Natural Science Foundation of China (81673359) and Sichuan Major Science and Technology Project on Biotechnology and Medicine (No. 2018SZDZX0018, China).

Author contributions

Wenhao Li took part in all work. Chuchu Zhou assisted in all experiments. Yao Fu was responsible for manuscript revision/review. Tijia Chen and Xing Liu assisted in animal experiments. Zhirong Zhang was responsible for funding and equipment support. Tao Gong was responsible for study concepts, experimental guidance, as well as funding and equipment support.

Conflicts of interest

All authors declare no conflicts of interest.

Appendix A. Supporting information

Supporting data to this article can be found online at https://doi.org/10.1016/j.apsb.2019.07.003.

References

1. Racanelli V, Rehermann B. The liver as an immunological organ. *Hepatology* 2006;**43**:S54−62.
2. Wang H, Thorling CA, Liang X, Bridle KR, Grice JE, Zhu Y, et al. Diagnostic imaging and therapeutic application of nanoparticles targeting the liver. *J Mater Chem B* 2015;**3**:939−58.
3. Pond SM, Tozer TN. First-pass elimination. Basic concepts and clinical consequences. *Clin Pharmacokinet* 1984;**9**:1−25.
4. Ghibellini G, Leslie EM, Brouwer KL. Methods to evaluate biliary excretion of drugs in humans: an updated review. *Mol Pharm* 2006;**3**:198−211.
5. Hoekstra LT, de Graaf W, Nibourg GA, Heger M, Bennink RJ, Stieger B, et al. Physiological and biochemical basis of clinical liver function tests. *Ann Surg* 2013;**257**:27−36.
6. Bertrand N, Leroux JC. The journey of a drug−carrier in the body: an anatomo-physiological perspective. *J Control Release* 2012;**161**:152−63.
7. Friedman SL. Hepatic stellate cells: protean, multifunctional, and enigmatic cells of the liver. *Physiol Rev* 2008;**88**:125−72.
8. Reddy LH, Couvreur P. Nanotechnology for therapy and imaging of liver diseases. *J Hepatol* 2011;**55**:1461−6.
9. Li L, Wang H, Ong ZY, Xu K, Ee PLR, Zheng S, et al. Polymer- and lipid-based nanoparticle therapeutics for the treatment of liver diseases. *Nano Today* 2010;**5**:296−312.
10. Fontana RJ, Goodman ZD, Dienstag JL, Bonkovsky HL, Naishadham D, Sterling RK, et al. Relationship of serum fibrosis markers with liver fibrosis stage and collagen content in patients with advanced chronic hepatitis C. *Hepatology* 2008;**47**:789−98.
11. Toffanin S, Friedman SL, Llovet JM. Obesity, inflammatory signaling, and hepatocellular carcinoma—an enlarging link. *Cancer Cell* 2010;**17**:115−7.
12. Jeng JE, Tsai JF, Chuang LY, Ho MS, Lin ZY, Hsieh MY, et al. Tumor necrosis factor-α 308.2 polymorphism is associated with advanced hepatic fibrosis and higher risk for hepatocellular carcinoma. *Neoplasia* 2007;**9**:987−92.
13. Fabregat I, Roncero C, Fernández M. Survival and apoptosis: a dysregulated balance in liver cancer. *Liver Int* 2007;**27**:155−62.
14. Friedman SL. Molecular regulation of hepatic fibrosis, an integrated cellular response to tissue injury. *J Biol Chem* 2000;**275**:2247−50.
15. Cheng Z, Lv Y, Pang S, Bai R, Wang M, Lin S, et al. Kallistatin, a new and reliable biomarker for the diagnosis of liver cirrhosis. *Acta Pharm Sin B* 2015;**5**:194−200.
16. Nagata K. Expression and function of heat shock protein 47: a collagen-specific molecular chaperone in the endoplasmic reticulum. *Matrix Biol* 1998;**16**:379−86.
17. Sauk JJ, Smith T, Norris K, Ferreira L. Hsp47 and the translation-translocation machinery cooperate in the production of alpha 1(I) chains of type I procollagen. *J Biol Chem* 1994;**269**:3941−6.
18. Friedman SL. Seminars in medicine of the Beth Israel Hospital, Boston. The cellular basis of hepatic fibrosis. Mechanisms and treatment strategies. *N Engl J Med* 1993;**328**:1828−35.
19. Iredale JP. Models of liver fibrosis: exploring the dynamic nature of inflammation and repair in a solid organ. *J Clin Investig* 2007;**117**:539−48.

20. Huang C, Zhang H, Bai R. Advances in ultrasound-targeted microbubble−mediated gene therapy for liver fibrosis. *Acta Pharm Sin B* 2017;**7**:447−52.
21. Schuppan D, Popov Y. Hepatic fibrosis: from bench to bedside. *J Gastroenterol Hepatol* 2002;**17 Suppl 3**:S300−5.
22. Hui AY, Friedman SL. Molecular basis of hepatic fibrosis. *Expert Rev Mol Med* 2003;**5**:1−23.
23. Yin C, Evason KJ, Asahina K, Stainier DY. Hepatic stellate cells in liver development, regeneration, and cancer. *J Clin Investig* 2013;**123**:1902−10.
24. Zhang X, Zhang Q, Peng Q, Zhou J, Liao L, Sun X, et al. Hepatitis B virus preS1-derived lipopeptide functionalized liposomes for targeting of hepatic cells. *Biomaterials* 2014;**35**:6130−41.
25. Liu R, Hu C, Yang Y, Zhang J, Gao H. Theranostic nanoparticles with tumor-specific enzyme- triggered size reduction and drug release to perform photothermal therapy for breast cancer treatment. *Acta Pharm Sin B* 2019;**9**:410−20.
26. Toole BP. Hyaluronan: from extracellular glue to pericellular cue. *Nat Rev Cancer* 2004;**4**:528−39.
27. Ossipov DA. Nanostructured hyaluronic acid-based materials for active delivery to cancer. *Expert Opin Drug Deliv* 2010;**7**:681−703.
28. Choi KY, Min KH, Na JH, Choi K, Kim K, Park JH, et al. Self-assembled hyaluronic acid nanoparticles as a potential drug carrier for cancer therapy: synthesis, characterization, and *in vivo* biodistribution. *J Mater Chem* 2009;**19**:4102−7.
29. Zhang Y, Sun T, Jiang C. Biomacromolecules as carriers in drug delivery and tissue engineering. *Acta Pharm Sin B* 2018;**8**:34−50.
30. Eliaz RE, Szoka FC. Liposome-encapsulated doxorubicin targeted to CD44 a strategy to kill CD44-overexpressing tumor cells. *Cancer Res* 2001;**61**:2592−601.
31. Sugahara KN, Murai T, Nishinakamura H, Kawashima H, Saya H, Miyasaka M. Hyaluronan oligosaccharides induce CD44 cleavage and promote cell migration in CD44-expressing tumor cells. *J Biol Chem* 2003;**278**:32259−65.
32. Zhong L, Xu L, Liu Y, Li Q, Zhao D, Li Z, et al. Transformative hyaluronic acid-based active targeting supramolecular nanoplatform improves long circulation and enhances cellular uptake in cancer therapy. *Acta Pharm Sin B* 2019;**9**:397−409.
33. Hu C, Cun X, Ruan S, Liu R, Xiao W, Yang X, et al. Enzyme-triggered size shrink and laser- enhanced NO release nanoparticles for deep tumor penetration and combination therapy. *Biomaterials* 2018;**168**:64−75.
34. Liu R, Xiao W, Hu C, Xie R, Gao H. Theranostic size-reducible and no donor conjugated gold nanocluster fabricated hyaluronic acid nanoparticle with optimal size for combinational treatment of breast cancer and lung metastasis. *J Control Release* 2018;**278**:127−39.
35. Smedsrod B. Cellular events in the uptake and degradation of hyaluronan. *Adv Drug Deliv Rev* 1991;**7**:265−78.
36. Laurent TC, Dahl IM, Dahl LB, Engström-Laurent A, Eriksson S, Fraser JR, et al. The catabolic fate of hyaluronic acid. *Connect Tissue Res* 1986;**15**:33−41.
37. Warren A, Bertolino P, Benseler V, Fraser R, McCaughan GW, Le Couteur DG. Marked changes of the hepatic sinusoid in a transgenic mouse model of acute immune-mediated hepatitis. *J Hepatol* 2007;**46**:239−46.
38. Chen YN, Hsu SL, Liao MY, Liu YT, Lai CH, Chen JF, et al. Ameliorative effect of curcumin-encapsulated hyaluronic acid-PLA nanoparticles on thioacetamide-induced murine hepatic fibrosis. *Int J Environ Res Public Health* 2017;**14**:11.
39. Zhu C, Gong S, Ding J, Yu M, Ahmad E, Feng Y, et al. Supersaturated polymeric micelles for oral silybin delivery: the role of the Soluplus−PVPVA complex. *Acta Pharm Sin B* 2019;**9**:107−17.
40. Cesur H, Rubinstein I, Pai A, Önyüksel H. Self-associated indisulam in phospholipid-based nanomicelles: a potential nanomedicine for cancer. *Nanomedicine* 2009;**5**:178−83.
41. Ashok B, Arleth L, Hjelm RP, Rubinstein I, Önyüksel H. *In vitro* characterization of PEGylated phospholipid micelles for improved drug solubilization: effects of PEG chain length and PC incorporation. *J Pharm Sci* 2004;**93**:2476−87.
42. Oh EJ, Park K, Kim KS, Kim J, Yang JA, Kong JH, et al. Target specific and long-acting delivery of protein, peptide, and nucleotide therapeutics using hyaluronic acid derivatives. *J Control Release* 2010;**141**:2−12.
43. Oh EJ, Kang SW, Kim BS, Jiang G, Cho IH, Hahn SK. Control of the molecular degradation of hyaluronic acid hydrogels for tissue augmentation. *J Biomed Mater Res* 2008;**86A**:685−93.
44. Jiang G, Park K, Kim J, Kim KS, Hahn SK. Target specific intracellular delivery of siRNA/PEI-HA complex by receptor mediated endocytosis. *Mol Pharm* 2009;**6**:727−37.
45. Luo Y, Prestwich GD. Synthesis and selective cytotoxicity of a hyaluronic acid-antitumor bioconjugate. *Bioconjug Chem* 1999;**10**:755−63.
46. Li J, Huo M, Wang J, Zhou J, Mohammad JM, Zhang Y, et al. Redox-sensitive micelles self-assembled from amphiphilic hyaluronic acid-deoxycholic acid conjugates for targeted intracellular delivery of paclitaxel. *Biomaterials* 2012;**33**:2310−20.
47. Song S, Chen F, Qi H, Li F, Xin T, Xu J, et al. Multifunctional tumor-targeting nanoparticles based on hyaluronic acid-mediated and pH-sensitive properties for efficient delivery of docetaxel. *Pharm Res* 2014;**31**:1032−45.
48. Li W, Yi X, Liu X, Zhang Z, Fu Y, Gong T. Hyaluronic acid ion-pairing nanoparticles for targeted tumor therapy. *J Control Release* 2016;**225**:170−82.
49. Zhang J, Wang W, Geng XH. The preparation and purification of silybin meglumine. *J Pharm Pract* 2008;**26**:274−7.
50. Xu P, Yin Q, Shen J, Chen L, Yu H, Zhang Z, et al. Synergistic inhibition of breast cancer metastasis by silibinin-loaded lipid nanoparticles containing TPGS. *Int J Pharm* 2013;**454**:21−30.
51. Raina K, Serkova NJ, Agarwal R. Silibinin feeding alters the metabolic profile in TRAMP prostatic tumors: ^{1}H-NMRS-based metabolomics study. *Cancer Res* 2009;**69**:3731−5.
52. Issa R, Zhou X, Constandinou CM, Fallowfield J, Millward-Sadler H, Gaca MD, et al. Spontaneous recovery from micronodular cirrhosis: evidence for incomplete resolution associated with matrix cross-linking. *Gastroenterology* 2004;**126**:1795−808.
53. Kim KS, Hur W, Park SJ, Hong SW, Choi JE, Goh EJ, et al. Bioimaging for targeted delivery of hyaluronic acid derivatives to the livers in cirrhotic mice using quantum dots. *ACS Nano* 2010;**4**:3005−14.
54. Hu CM, Zhang L, Aryal S, Cheung C, Fang RH, et al. Erythrocyte membrane-camouflaged polymeric nanoparticles as a biomimetic delivery platform. *Proc Natl Acad Sci U S A* 2011;**108**:10980−5.
55. Cao X, Luo J, Gong T, Zhang ZR, Sun X, Fu Y. Co-encapsulated doxorubicin and bromotetrandrine lipid nanoemulsions in reversing multidrug resistance in breast cancer *in vitro* and *in vivo*. *Mol Pharm* 2015;**12**:274−86.
56. Marumoto Y, Terai S, Urata Y, Matsumoto T, Mizunaga Y, Yamamoto N, et al. Continuous high expression of XBP1 and GRP78 is important for the survival of bone marrow cells in CCl_4-treated cirrhotic liver. *Biochem Biophys Res Commun* 2008;**367**:546−52.
57. Zhou J, Zhang X, Li M, Wu W, Sun X, Zhang L, et al. Novel lipid hybrid albumin nanoparticle greatly lowered toxicity of pirarubicin. *Mol Pharm* 2013;**10**:3832−41.
58. Khatik R, Dwivedi P, Shukla A, Srivastava P, Rath SK, Paliwal SK, et al. Development, characterization and toxicological evaluations of

phospholipids complexes of curcumin for effective drug delivery in cancer chemotherapy. *Drug Deliv* 2016;**23**:1067−78.
59. Li M, Tang Z, Lv S, Song W, Hong H, Jing X, et al. Cisplatin crosslinked pH-sensitive nanoparticles for efficient delivery of doxorubicin. *Biomaterials* 2014;**35**:3851−64.
60. Poelstra K, Prakash J, Beljaars L. Drug targeting to the diseased liver. *J Control Release* 2012;**161**:188−97.
61. Bartsch M, Weeke-Klimp AH, Meijer DK, Scherphof GL, Kamps JA. Massive and selective delivery of lipid-coated cationic lipoplexes of oligonucleotides targeted *in vivo* to hepatic endothelial cells. *Pharm Res* 2002;**19**:676−80.
62. Duan R, Sun X, Liu J, Gong T, Zhang Z. Mixed micelles loaded with silybin-polyene phosphatidylcholine complex improve drug solubility. *Acta Pharmacol Sin* 2011;**32**:108−15.
63. Yue J, Wang R, Liu S, Wu S, Xie Z, Huang Y, et al. Reduction-responsive shell-crosslinked micelles prepared from Y-shaped amphiphilic block copolymers as a drug carrier. *Soft Matter* 2012;**8**:7426−35.
64. Talelli M, Morita K, Rijcken CJ, Aben RW, Lammers T, Scheeren HW, et al. Synthesis and characterization of biodegradable and thermosensitive polymeric micelles with covalently bound doxorubicin-glucuronide prodrug *via* click chemistry. *Bioconjug Chem* 2011;**22**:2519−30.